Co-deposition growth and superconductivity of $La_{2-x}Sr_xCuO_4$ films by reactive molecular beam epitaxy

Yang Wang,[1,*] Rui-Feng Wang,[1,*] Qinghua Zhang,[2] Menghan Liao,[1] Lin Gu,[2] Ding Zhang,[1,3,4] Can-Li Song,[1,3,†] Xu-Cun Ma,[1,3,‡] and Qi-Kun Xue[1,3,4,5]

[1]*State Key Laboratory of Low-Dimensional Quantum Physics, Department of Physics, Tsinghua University, Beijing 100084, China*

[2]*Institute of Physics, Chinese Academy of Sciences, Beijing 100190, China*

[3]*Frontier Science Center for Quantum Information, Beijing 100084, China*

[4]*Beijing Academy of Quantum Information Sciences, Beijing 100193, China*

[5]*Southern University of Science and Technology, Shenzhen 518055, China*

(Received 11 January 2021; revised 19 April 2021; accepted 11 May 2021; published 24 May 2021)

Reactive molecular beam epitaxy has been employed to prepare $La_{2-x}Sr_xCuO_4$ cuprate films via a Co-deposition method. Precise control of flux ratios among the solid sources leads us to establish a very narrow growth window for the cation stoichiometry. The hole doping by divalent Sr^{2+} cation is found to occur in a substitution-limited manner, accompanied by partial oxidation of Sr flux into peroxide SrO_2 on the top surface. Through interface engineering, we explore the impact of substrate strain on the crystal parameters and superconductivity of $La_{2-x}Sr_xCuO_4$ thin films. The present study provides a time-saving, effective approach to preparing high-quality cuprate films, and further understanding the effect of surface/interface microstructures on cuprate superconductivity.

DOI: 10.1103/PhysRevB.103.184514

I. INTRODUCTION

Since the discovery of high-temperature (T_c) superconductivity in a La-Ba-Cu-O compound [1], an increasing number of cuprate compounds have been synthesized and investigated, aiming at unveiling the secret of this macroscopic quantum phenomenon [2,3]. To date, a complicated phase diagram of cuprates with various competing orders [4–7] has been established, but the microscopic mechanism of high-T_c superconductivity remains mysterious. Compared to many bulk techniques, the surface-sensitive measurements via scanning tunneling microscopy (STM) display unique advantages in characterizing the novel properties of cuprates, such as nanoscale electronic inhomogeneity, charge orders, and nematicity [8–10]. These indispensable real-space observations have largely contributed to understanding the pairing mechanism of high-T_c superconductivity in cuprates. Unfortunately, this technique has been limited to a tiny group of cleavable cuprate superconductors such as $Bi_2Sr_2CaCu_2O_{8+\delta}$ and $YBa_2Cu_3O_{7-\delta}$ [11]. To overcome this obstacle, epitaxial cuprate films are desired and serve as an alternative platform for extending the STM measurements to other cuprate superconductors.

The canonical cuprate compound $La_{2-x}Sr_xCuO_4$ (LSCO) has attracted increasing attention over the past 30 years, in terms of its relatively simple crystal structure, well-documented charge order, and superconductivity phase diagram [12–14]. However, the LSCO crystals are not easily cleavable, impeding a systematic STM study on their bulk counterparts [15,16]. Atomic-layer-by-layer deposition (ALL) has been developed to prepare LSCO epitaxial thin films, superlattices and intercalated monolayer with specific doping [17–21]. However, ALL is often a time-consuming method and demands precise calibration of absolute deposition rates for each element involved [17,22]. Moreover, it is hard to combine STM with ALL, because the strict vibration isolation for STM is incompatible with the turbulent vacuum-pumping equipment demanded for ALL. On the other hand, as a thermodynamically stable phase, epitaxial LSCO films can be prepared more efficiently via a Co-deposition process, which only needs control of the relative deposition rates of relevant elements [17]. Here we combine a reactive ozone-assisted molecular beam epitaxy (MBE) and an *in situ* STM to optimize the co-deposition growth of LSCO films on two types of substrates, and establish a time-saving and effective method for preparing high-quality cuprate films.

II. EXPERIMENT

Our experiments were conducted in an ultrahigh vacuum (UHV) MBE-STM combined system (Unisoku) with a base pressure better than 2.0×10^{-10} Torr. The Nb-doped $SrTiO_3$ (STO, 0.05 wt.%) substrates were cleaned at 1200°C for 10 min. to obtain the TiO_2-terminated surface and held at 700°C during the film growth, while the insulating $LaSrAlO_4$ (LSAO) substrates were heated in a tube furnace at 900°C for 2 h to obtain an atomically flat surface before being transferred into UHV [23]. Epitaxial $La_{2-x}Sr_xCuO_4$ thin films were prepared by co-evaporating high-purity Cu (99.9999%), La (99.9%), and Sr (99.95%) sources from their respective

*These authors contributed equally to this work.
†clsong07@mail.tsinghua.edu.cn
‡xucunma@mail.tsinghua.edu.cn

effusion cells under an ozone pressure of 1.5×10^{-5} Torr. Prior to the Co-deposition growth, the flux of each source was calibrated by a quartz crystal microbalance (QCM, Inficon SQM160H). The thickness of all epitaxial films was fixed to 10 unit cells. Once the film growth was terminated, the samples were *in situ* transferred into the STM chamber for data collection at 4.2 K. Polycrystalline PtIr tips were conditioned by electron beam bombardments and appropriately calibrated on MBE-grown Ag/Si (111) films before the STM measurements in a constant-current mode. The samples were then transferred out of UHV for x-ray diffraction (XRD), scanning transmission electron microscopy (STEM), transport measurements and so on.

III. RESULT AND DISCUSSION

We began with the search of optimal growth conditions for stoichiometric La_2CuO_4 (La-214) thin films by delicately adjusting the flux ratio between La and Cu sources. As the La:Cu flux ratio increases from 1:1 to 2:1, a structural transition from $LaCuO_3$ (La-113) phase [Fig. 1(a)] to La-214 phase [Fig. 1(b)] occurs and is unambiguously confirmed by our XRD measurements in Fig. 1(c). The XRD diffraction peaks are initially characteristic of the pure La-113 phase at La:Cu = 1.0, and eventually the La-214 phase at La:Cu $\approx$ 2.0, while a mixture of the two phases exists in the immediate flux ratio of La:Cu. In what follows, the epitaxial Co-deposition growth of doped $La_{2-x}Sr_xCuO_4$ films was performed with varying flux ratios of Sr:Cu under an appropriate La:Cu ratio. By carefully characterizing the surface structure for a vast number of LSCO samples, a growth phase diagram is established in Fig. 1(d). Evidently, the growth window for single-phase and stoichiometric LSCO films (part of the $\sqrt{2}\times\sqrt{2}$ area in the phase diagram) is extremely narrow, indicating that a careful tuning of the flux ratios among the solid sources is the key to prepare high-quality films. Note that various charge orders have been observed in the epitaxial LSCO thin films, as well documented before [24] and summarized in the phase diagram. The superstructure changes with the Sr concentration and displays a systematic evolution from a Wigner crystal phase to an incommensurate or commensurate stripe phase, a $\sqrt{2}\times\sqrt{2}$ reconstructed phase, and finally a grid phase. It is worth noting that two and more superstructures coexist near the boundaries between various phases, due to spontaneous phase separation on the surface.

It should be emphasized that the flux ratios reported here refers to those measured by QCM at room temperature, rather than the actual stoichiometry of epitaxial films. Judging from the growth condition $T_{La,Cu} \gg T_{Sub} \gg T_{Sr}$, where T_{La}, T_{Cu}, T_{Sr} and $T_{Sub} = 700^{o}$C are the temperatures of La, Cu, Sr cells and substrate, respectively, the sticking coefficients for La and Cu are very close to unity. In contrast, the majority of Sr would be either desorbed from the heated STO substrate or oxidized by ozone. Consequently, the actual substitution

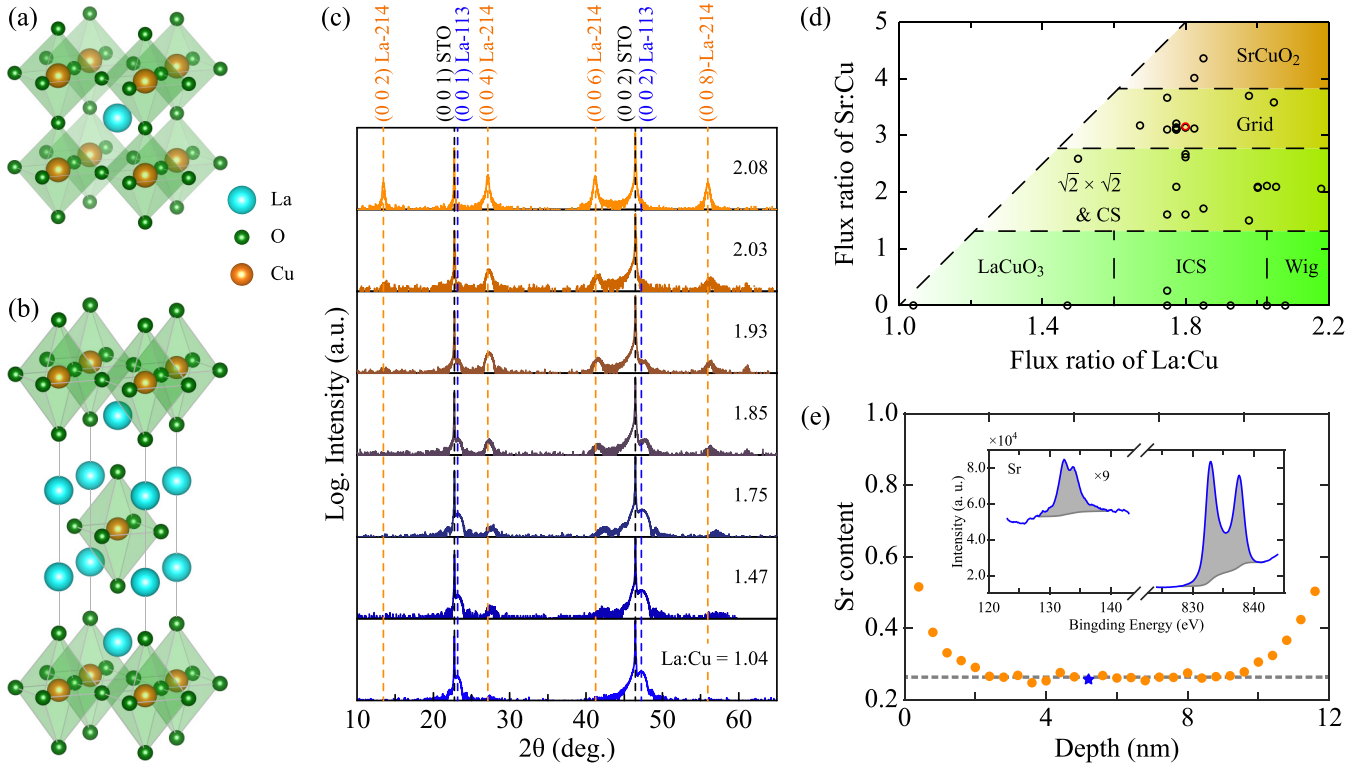

FIG. 1. (a), (b) Crystal structures of La-113 and La-214 phases. (c) A series of XRD patterns of La-214 epitaxial films with increasing La:Cu flux ratio indicated. Dashed lines mark the Brag peak positions for different phases, respectively. (d) Phase diagram of La-Sr-Cu-O films. The circles represent all samples explored to determine the phase diagram, while the red circle marks the sample measured by XPS in (e). (e) Depth-dependent Sr content measured by XPS. The dashed line marks the mean Sr content in the bulk part of the epitaxial film. Inset displays XPS intensity at the binding energy of $3d_{3/2}$, $3d_{5/2}$ orbits of Sr (magnified nine times for clarity) and $3d_{5/2}$ orbit of La, which is used to determine the Sr content at the depth of 5 nm (marked by the blue pentagram).

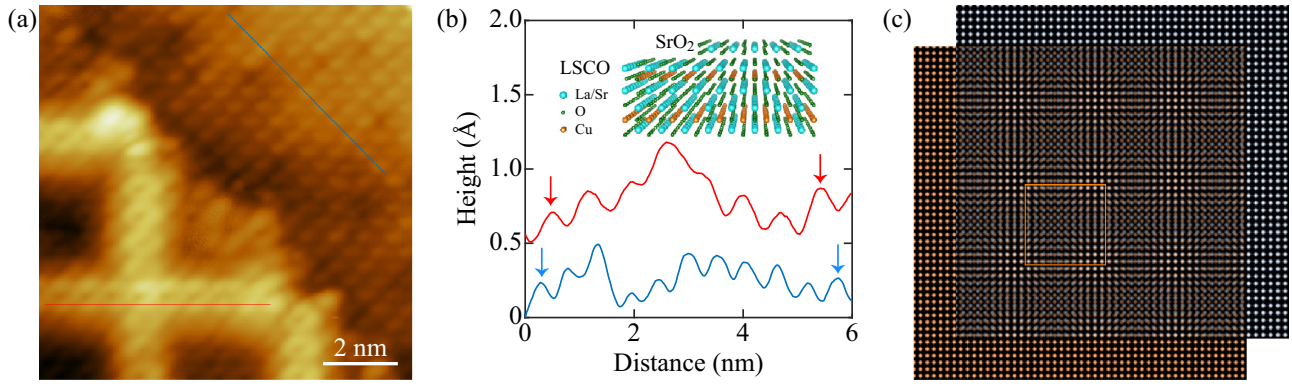

FIG. 2. (a) STM topography (10 nm×10 nm, $V = -1.6$ V, $I = 20$ pA) with coexisting $\sqrt{2}\times\sqrt{2}$ phase and grid phase. (b) Line profiles along the blue and red lines in (a), showing different lattice constants of the $\sqrt{2}\times\sqrt{2}$ phase and the grid phase. For clarity, the red line in (a) runs along the 45° direction with respect to the nearest neighbor bright spots. The peak distance of the blue profile (5.44 Å) matches $\sqrt{2}$ times of the La-La spacing of LSCO, while the peak distance of the red line profile (7.08 Å) matches two times of the Sr-Sr spacing in SrO_2. The inset illustrates a schematic diagram of the SrO_2 overlayer on LSCO. (c) Simulated Moiré pattern between the SrO_2 plane (orange) and LaO plane (white). The orange square denotes the unit cell of gridlike superstructure.

of divalent Sr^{2+} for trivalent La^{3+} is far below the nominal flux ratio measured by QCM. In other words, the hole doping level by Sr^{2+} should be substitution-limited in the LSCO films, due to the higher T_{Sub} of 700°C used. Such a substitution-limited manner has been actually confirmed by measuring the doping level via x-ray photoelectron spectroscopy (XPS). Plotted in Fig. 1(e) is the XPS measurement from an LSCO/STO sample with a nominal flux ratio of Sr:Cu = 3.2. By calculating the XPS intensities of La $3d_{5/2}$, Sr $3d_{3/2}$ and $3d_{5/2}$, the Sr:La stoichiometry is estimated to be only 0.26, which is significantly smaller than the nominal flux ratio of 3.2. It is worth noting that the concentration of Sr increases appreciably at the bottom and top of LSCO films in Fig. 1(e). This could be easily accounted for by the permeation of Sr from the underlying STO substrate, as well as some remanent Sr or strontium oxides on the top surface.

Indeed, monolayer strontium peroxide (SrO_2) is evidenced from a careful analysis of the STM image on the grid phase [Fig. 2(a)], which always occurs at high Sr flux and has been previously interpreted as crossed vertical and horizontal stripes before [24]. A closer examination of atomically resolved STM topography with coexisting grid phase and LSCO-($\sqrt{2}\times\sqrt{2}$) reconstructed surface reveals the nature of grid phase as SrO_2, resembling that of $Sr_{1-x}Nd_xCuO_2$ films in a prominent way [25]. A minor but critical difference is the larger spacing of ~4.3 nm for the superstructure in LSCO than that (~3.5 nm) in $Sr_{1-x}Nd_xCuO_2$. By taking the line profiles along the high-symmetry directions in Fig. 2(b), the in-plane lattice parameters are measured to be 5.44 Å for the $\sqrt{2}\times\sqrt{2}$ phase and 5.01 Å for the grid phase, respectively. The apparent deviation of lattice parameters implies the different nature of the two exposed surfaces. The spacing of 5.44 Å matches excellently with the $\sqrt{2}$ times of La-La distance (3.85 Å) on LaO surface, while the value of 5.01 Å/$\sqrt{2} = 3.54$ Å is almost the lattice constant of the peroxide SrO_2 (3.55 Å) [26]. By overlapping the two lattices of SrO_2 and LaO, a Moiré pattern with a periodicity of 4.40 nm is observed in Fig. 2(c) and is consistent with the periodicity of the gridlike superstructure. We thus conclude that the grid phase stems from the oxidation of partial Sr into SrO_2 on the surface.

Our fine tuning of the flux ratio establishes a co-deposition growth window for stoichiometric LSCO cuprate, but the epitaxial films exhibit no superconductivity due to the strain imposed by the substrates. For STO with in-plane lattice constants 3% larger than LSCO, the large tensile strain at the interface prevents the superconductivity [27]. Alternatively, the LSAO has a smaller lattice constant (0.375 nm) than LSCO, and thus imposes a slight compressive interfacial strain, which was reported to be beneficial to the superconductivity of LSCO films [27–30]. We thus prepare LSCO films by employing the above-established growth recipe. Figure 3(a) shows a representative XRD pattern of an LSCO film on the LSAO substrate. The sharp diffraction peaks justify the high quality of epitaxial LSCO films, indicative of the generic applicability of epitaxial Co-deposition growth. The interface between LSCO and LSAO is then examined by a high-resolution STEM measurement, as illustrated in Fig. 3(b). The sharp interface shows a stacking sequence of AlO_2-LaO-AlO_2-LaO-LaO-CuO_2-LaO in the direction from the substrate to the film. Conversely, there always exists a spontaneously formed $LaCuO_3$ buffer layer with a thickness of 4-5 unit cells separating the STO substrates and LSCO films, even though a flux ratio of La:Cu = 2:1 is satisfied [24]. Apparently, the lattice-matching LSAO substrate plays an important role in guaranteeing a perfect interface for epitaxial LSCO films. Another distinction between the LSAO and STO substrates is the c-lattice constants of LSCO films grown on them. As shown in Fig. 3(c), larger c-lattice constants around 13.25 Å are observed in LSCO/LASO than those ~13.10 Å in LSCO/STO. The c-axis lattice parameter somewhat increases with Sr content as Sr:Cu < 3, which is more clearly manifested in LSCO/STO, and then shrinks a little beyond Sr:Cu ~3. These results qualitatively match the previously reported data of LSCO/LSAO films, in which the c-axis lattice parameter increases at the underdoped regime but decreases at the overdoped regime [31,32]. A possible reason for the increase of c at low Sr content is due to the larger ionic radius of Sr^{2+} (1.44 Å) than that of La^{3+} (1.36 Å) [33],

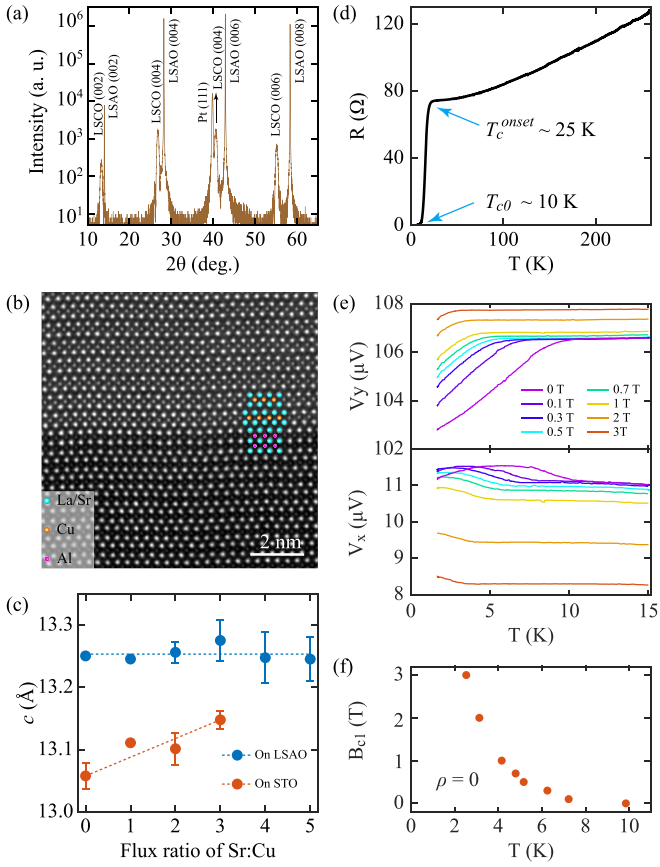

FIG. 3. (a) XRD pattern of the LSCO film grown on the Pt electrode prepatterning LSAO substrate. The brag peaks from the LSCO film, LSAO substrate, and Pt electrode are all evident. (b) STEM image of the LSCO/LSAO interface showing a sharp interface. For clarity, color-coded atoms matching with the experimental observations are partly superimposed on the image. (c) Comparison of the c-axis lattice parameters of LSCO thin films grown on LSAO and STO substrates at varied flux ratios of Sr:Cu. The dashed lines are guide to eyes. Many similar samples are averaged and the error bars represent the standard deviations. (d) Resistance *vs* temperature curve showing superconductivity of the LSCO/LSAO sample with an onset temperature T_c^{onset} around 25 K and zero-resistivity temperature T_{c0} around 10 K. (e) Imaginary parts (upper panel) and real parts (lower panel) of mutual inductance as a function of temperature under a series of magnetic fields. (f) The Meissner fields B_{c1} of LSCO at different temperatures. The data are extracted from the inflection points of V_y vs T curves in (e).

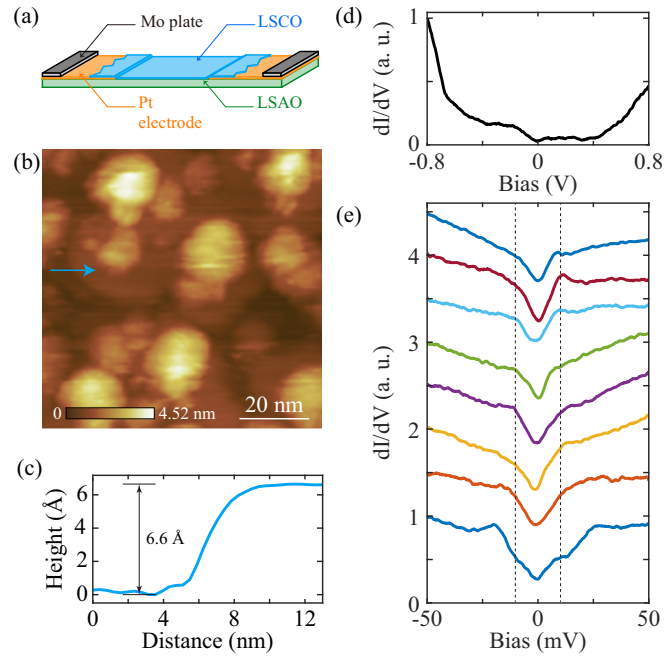

FIG. 4. (a) Schematic diagram of the setup of LSCO film grown on the Pt electrode prepatterning LSAO substrate. The Pt electrodes are used to connect the LSCO film and Mo plates of the sample holder. (b) STM topography (80 nm × 80 nm, $V = -5$ V, $I = 10$ pA) of the LSCO/LSAO sample with preprepared Pt electrodes. (c) Line profile along the blue arrow in (b). (d) Large-energy-scale dI/dV spectrum (setpoints: $V = -1$ V, $I = 200$ pA) in the LSCO/LSAO film. (e) Low-energy-scale dI/dV spectra (setpoints: $V = -50$ mV, $I = 200$ pA) of the LSCO/LSAO film. All the spectra in (d) and (e) are measured on the flat terraces. The dashed lines denote the average energy of the spectral kinks.

while the decrease of c at high Sr content calls for further investigation. The LSCO films grown on LSAO substrates are confirmed to be superconducting by the transport measurements. The LSCO films with Sr composition $x = 0.22$ exhibit a clear superconducting transition with an onset temperature $T_c^{\text{onset}} \sim 25$ K and zero-resistivity temperature $T_{c0} \sim 10$ K. [Fig. 3(d)]. And the measurement of mutual inductance also shows evident superconducting transition below T_{c0} [Fig. 3(e)]. By extracting the inflection points under various magnetic fields, we illustrate the relationship between Meissner field (B_{c1}) and temperature [Fig. 3(f)], which exhibits an expected behavior of $d^2B_{c1}/dT^2 > 0$ in LSCO samples [34]. These results compellingly demonstrate that the Co-deposition growth is a time-saving and effective approach to preparing superconducting LSCO films.

Another remarkable advantage of the epitaxial Co-deposition growth is its direct compatibility to an *in situ* STM study. However, the insulating LSAO substrate prevents us from readily probing the superconducting LSCO samples. To overcome this issue, we deposit Pt electrodes through a mask on the LSAO substrates before the MBE growth [Fig. 4(a)], so that the bias voltage could be applied to the superconducting LSCO films. Figure 4(b) displays an STM topography of the LSCO films on LSAO. Unfortunately, the surface is covered by many nanosized bright clusters, probably caused by the migration and/or reaction of Pt atoms during the MBE growth. Some flat terraces with sharp edges still occur, separated by a half unit-cell step height (~6.6 Å) of LSCO [Fig. 4(c)]. The conductance spectra are also measured in the flat terraces. The spectrum in the large energy range [Fig. 4(d)] exhibits similar features with some prototypical hole-doped cuprates [35,36], including the similar particle-hole asymmetry and a dip near the zero bias. The low-energy spectra near the Fermi energy show relatively robust kinks at ±10 mV, which is consistent with the previously reported superconducting gap in both bulk and film samples of LSCO [15,16,37]. Combined with the inspection of superconductivity by transport measurements [Figs. 3(d) and 3(e)], these spectra should reflect the

superconducting properties of the *in situ* LSCO/LSAO thin film.

IV. SUMMARY

In summary, the epitaxial Co-deposition growth approach has been demonstrated and could serve as an effective method for preparing LSCO films, and by implication, for other non-cleavable cuprate films. Through a precise control of flux ratios and interface engineering, we succeed in preparing superconducting LSCO films and establish their very narrow growth windows. Moreover, we reveal the substitution-limited manner of Sr^{2+} doping, strain effects on the interface structure, and electronic properties of LSCO films.

ACKNOWLEDGMENTS

We thank K.-L. Jiang's group for assisting the preparation of the Pt electrode prepatterning LSAO substrates. This work is financially supported by the National Natural Science Foundation of China (Grants No. 51788104, No. 11774192, and No. 11634007), the Ministry of Science and Technology of China, and the Beijing Advanced Innovation Center for Future Chip (ICFC).

[1] J. G. Bednorz and K. A. Müller, Z. Phys. B **64**, 189 (1986).
[2] C. Chu, L. Deng, and B. Lv, Physica C **514**, 290 (2015).
[3] N. P. Armitage, P. Fournier, and R. L. Greene, Rev. Mod. Phys. **82**, 2421 (2010).
[4] B. Keimer, S. A. Kivelson, M. R. Norman, S. Uchida, and J. Zaanen, Nature (London) **518**, 179 (2015).
[5] M. Hashimoto, I. M. Vishik, R.-H. He, T. P. Devereaux, and Z.-X. Shen, Nat. Phys. **10**, 483 (2014).
[6] R. Comin and A. Damascelli, Annu. Rev. Condens. Matter Phys. **7**, 369 (2016).
[7] J. Tranquada, B. Sternlieb, J. Axe, Y. Nakamura, and S. Uchida, Nature (London) **375**, 561 (1995).
[8] S. H. Pan, J. O'neal, R. Badzey, C. Chamon, H. Ding, J. Engelbrecht, Z. Wang, H. Eisaki, S. Uchida, A. Gupta *et al.*, Nature (London) **413**, 282 (2001).
[9] T. Hanaguri, C. Lupien, Y. Kohsaka, D.-H. Lee, M. Azuma, M. Takano, H. Takagi, and J. Davis, Nature (London) **430**, 1001 (2004).
[10] A. Schmidt, K. Fujita, E. Kim, M. Lawler, H. Eisaki, S. Uchida, D. Lee, and J. Davis, New J. Phys. **13**, 065014 (2011).
[11] Ø. Fischer, M. Kugler, I. Maggio-Aprile, C. Berthod, and C. Renner, Rev. Mod. Phys. **79**, 353 (2007).
[12] J.-M. Tarascon, L. Greene, W. McKinnon, G. Hull, and T. Geballe, Science **235**, 1373 (1987).
[13] T. P. Croft, C. Lester, M. S. Senn, A. Bombardi, and S. M. Hayden, Phys. Rev. B **89**, 224513 (2014).
[14] S. Badoux, S. A. A. Afshar, B. Michon, A. Ouellet, S. Fortier, D. LeBoeuf, T. P. Croft, C. Lester, S. M. Hayden, H. Takagi, K. Yamada, D. Graf, N. Doiron-Leyraud, and L. Taillefer, Phys. Rev. X **6**, 021004 (2016).
[15] T. Kato, S. Okitsu, and H. Sakata, Phys. Rev. B **72**, 144518 (2005).
[16] N. Momono, T. Kurosawa, T. Endo, K. Kurusu, K. Takeyama, M. Oda, and M. Ido, J. Phys. Chem. Solids **69**, 3031 (2008).
[17] I. Božović, IEEE Trans. Appl. Supercond. **11**, 2686 (2001).
[18] I. Božović, X. He, J. Wu, and A. Bollinger, Nature (London) **536**, 309 (2016).
[19] A. Gozar, G. Logvenov, L. F. Kourkoutis, A. Bollinger, L. Giannuzzi, D. Muller, and I. Božović, Nature (London) **455**, 782 (2008).
[20] G. Logvenov, A. Gozar, and I. Božović, Science **326**, 699 (2009).
[21] A. Suter, E. Morenzoni, T. Prokscha, B. M. Wojek, H. Luetkens, G. Nieuwenhuys, A. Gozar, G. Logvenov, and I. Božović, Phys. Rev. Lett. **106**, 237003 (2011).
[22] I. Božović, J. Eckstein, G. Virshup, A. Chaiken, M. Wall, R. Howell, and M. Fluss, J. Supercond. **7**, 187 (1994).
[23] A. Biswas, P. Rossen, J. Ravichandran, Y.-H. Chu, Y.-W. Lee, C.-H. Yang, R. Ramesh, and Y. Jeong, Appl. Phys. Lett. **102**, 051603 (2013).
[24] Y. Wang, Y. Zhong, Z. Luo, M. Liao, R. Wang, Z. Dou, Q. Zhang, D. Zhang, L. Gu, C.-L. Song *et al.*, npj Quantum Mater. **4**, 1 (2019).
[25] J.-Q. Fan, S.-Z. Wang, X.-Q. Yu, R.-F. Wang, Y.-L. Xiong, C.-L. Song, X.-C. Ma, and Q.-K. Xue, Phys. Rev. B **101**, 180508(R) (2020).
[26] S. C. Middleburgh, K. P. D. Lagerlof, and R. W. Grimes, J. Am. Ceram. Soc. **96**, 308 (2013).
[27] I. Božović, G. Logvenov, I. Belca, B. Narimbetov, and I. Sveklo, Phys. Rev. Lett. **89**, 107001 (2002).
[28] W. Si and X. Xi, Appl. Phys. Lett. **78**, 240 (2001).
[29] H. Sato and M. Naito, Physica C **274**, 221 (1997).
[30] W. Si, H.-C. Li, and X. Xi, Appl. Phys. Lett. **74**, 2839 (1999).
[31] E. Stilp, A. Suter, T. Prokscha, E. Morenzoni, H. Keller, B. M. Wojek, H. Luetkens, A. Gozar, G. Logvenov, and I. Božović, Phys. Rev. B **88**, 064419 (2013).
[32] G. Logvenov, I. Sveklo, and I. Božović, Physica C **460**, 416 (2007).
[33] R. D. Shannon, Acta Cryst. A **32**, 751 (1976).
[34] X. Shi, P. V. Lin, T. Sasagawa, V. Dobrosavljević, and D. Popović, Nat. Phys. **10**, 437 (2014).
[35] P. Cai, W. Ruan, Y. Peng, C. Ye, X. Li, Z. Hao, X. Zhou, D.-H. Lee, and Y. Wang, Nat. Phys. **12**, 1047 (2016).
[36] Y. Kohsaka, T. Hanaguri, M. Azuma, M. Takano, J. Davis, and H. Takagi, Nat. Phys. **8**, 534 (2012).
[37] O. Yuli, I. Asulin, O. Millo, and G. Koren, Phys. Rev. B **75**, 184521 (2007).